Analysis of Shear Wave Propagation derived from MR Elastography in 3D Thigh Skeletal Muscle using Subject Specific Finite Element Model

Tien Tuan Dao, Philippe Pouletaut, Fabrice Charleux, Marie-Christine Ho Ba Tho, and Sabine Bensamoun

Abstract— **The purpose of this study was to develop a subject specific finite element model derived from MRI images to numerically analyze the MRE (magnetic resonance elastography) shear wave propagation within skeletal thigh muscles. A sagittal T2 CUBE MRI sequence was performed on the 20-cm thigh segment of a healthy male subject. Skin, adipose tissue, femoral bone and 11 muscles were manually segmented in order to have 3D smoothed solid and meshed models. These tissues were modeled with different constitutive laws. A transient modal dynamics analysis was applied to simulate the shear wave propagation within the thigh tissues. The effects of MRE experimental parameters (frequency, force) and the muscle material properties (shear modulus: C_{10}) were analyzed through the simulated shear wave displacement within the vastus medialis muscle. The results showed a plausible range of frequencies (from 90Hz to 120 Hz), which could be used for MRE muscle protocol. The wave amplitude increased with the level of the force, revealing the importance of the boundary condition. Moreover, different shear displacement patterns were obtained as a function of the muscle mechanical properties. The present study is the first to analyze the shear wave propagation in skeletal muscles using a 3D subject specific finite element model. This study could be of great value to assist the experimenters in the set-up of MRE protocols.**

I. Introduction

Biological tissues are commonly altered during pathophysiological process. The early depiction of their abnormal behaviors in a non-invasive manner remained a challenge in the medical field. Recently, magnetic resonance elastography (MRE) has been widely used to assess *in vivo* viscoelastic properties of different biological tissues such as the liver [1], the brain [2] or the skeletal muscle [3]. Actually, MRE liver test is performed in clinical practice enabling the diagnosis of the fibrosis stage and the evaluation of the clinical treatment.

However, the development of MRE technique for the characterization of skeletal muscles remained a challenge due to theoretical and experimental issues. From an anatomical point of view, the muscle can be superficially or deeply localized, and its multi scale architecture revealed a complex living material (anisotropic, heterogeneous, etc…). This behavior is emphasized for pathological muscles due to the changes [4]. MRE protocol performed on muscle is composed of a mechanical excitation, a pneumatic driver and an ergometer device in order to determine the muscle behavior in passive and active conditions. Thus, shear waves are generated within the muscle of interest, with optimal experimental MRE parameters (burst count, frequency, force, etc…). Subsequently, the analysis of the shear wave displacement in muscle tissue volume allows the measurement of the mechanical properties (i.e. shear modulus, viscosity) of the muscle [3-4].

The optimization of this muscle experimental set-up is extremely time-consuming and many repetitive trials are necessary to find the optimal MRE parameters. Thus, a computer-aided design (CAD) [5], such as finite element modeling, could allow MRE experimenters to reduce significantly efforts. However, this numerical approach needs to take the architecture and the complex behavior of the skeletal muscles into account to accurately analyze their mechanical responses. Medical imaging techniques (magnetic resonance imaging (MRI) or computed tomography) revealed the structural properties of the tissue and have been used to develop accurate finite element models of the musculoskeletal system [6].

Thus, the present study aimed at developing a subject specific finite element model derived from MRI images to numerically analyze the MRE shear wave propagation within skeletal thigh muscles. This model was applied to the vastus medialis muscle and could be of great value to assist the experimenters in the set-up of MRE protocols.

II. Materials and Methods

A. MRI Data Acquisition

A sagittal T2 CUBE MRI (1.5T, Signa HDx, GE) sequence was performed in the lower third part of the thigh due to the low amount of adipose tissue. Thus, 20 cm thigh segment was scanned in a healthy 33-year-old male subject (body mass index: 22.9 kg/m²) at the Polyclinique Saint Côme (Compiègne, France), and informed consent was signed before the data acquisition. The pixel matrix was 512 x 512, the slice thickness was 1mm, the echo and repetition times were 30 ms and 2200 ms, respectively.

B. Image-based finite element modeling

i) Image processing and Mesh generation

Manual segmentation was applied on all MRI images to separate the skin, femoral bone, the adipose tissue and 11 thigh muscles using ScanIP software (Simpleware, Exeter,

T.T. Dao, P. Pouletaut, M.C. Ho Ba Tho, S.F. Bensamoun are with the UMR CNRS 7338 - Biomechanics and Bioengineering, University of Technology of Compiegne, BP 20529, 60205 Compiègne cedex, France (Corresponding author: 33 3 44 23 43 34/tien-tuan.dao@utc.fr).

F. Charleux is with ACRIM-Polyclinique St Côme, BP 70409 - 60204, Compiègne Cedex, France.

978-1-4244-7929-0/14/$26.00 ©2014 IEEE

UK). Subsequently, the thigh geometry was divided in 14 regions corresponding to the femoral bone, the adipose tissue composed of the aponorosis between the muscles and the fat, the skin surrounding the thigh, and the 11 muscles (Fig. 1).

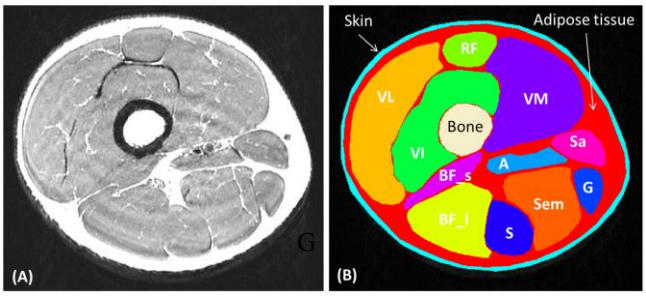

Figure 1. MRI anatomical (A) and segmented (B) images including 14 regions of the thigh: femoral bone, skin, adipose tissue, and 11 muscles (Rectus Femoris (RF), Vastus Lateralis (VL), Vastus Medialis (VM), Vastus Intermedius (VI), Biceps Femoris (Short Head) (BF_s), Biceps Femoris (Long Head) (BF_l), Semitendinosus (S), Semimembranosus (Sem), Adductor (A), Sartorius (Sa), Gracilis (G)).

A 'home-made' developed process [7] was applied to create 3D smoothed solid and meshed models of four regions composed of the skin, the femoral bone, the investigated vastus medialis muscle and the ten remaining muscles grouped with the adipose tissue (Fig. 2A). The mesh was composed of 4-node linear tetrahedron, hybrid, linear pressure elements (3D-tetrahedra C3D4H) and the element size was 5 x 5 x 5 mm^3 (Fig 2B). The skin model had 6111 nodes and 17914 elements. The vastus medialis muscle model had 5184 nodes and 24802 elements. The femoral bone model had 2049 nodes and 9224 elements. The group of adipose tissue and other muscles was made with 20847 nodes and 105031 elements.

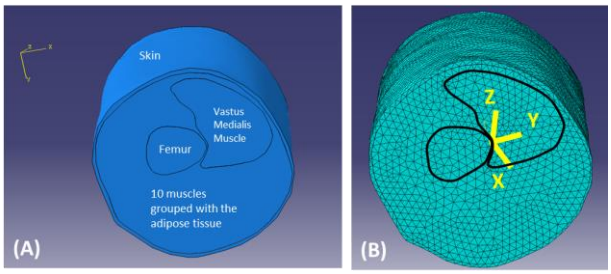

Figure 2. Solid (A) and meshed (B) models of the thigh structures.

ii) Material constitutive laws

Different constitutive laws (Table I) were applied to model the four regions of the thigh. Thus, the femoral bone was modeled with a linear elastic and isotropic behavior while the adipose tissue was represented by a nonlinear hyperelastic Mooney-Rivlin law. The skin and all the muscles were modeled with Neo-Hookean behaviors. Subsequently, the corresponding mechanical properties obtained from the literature for these different materials were used as input values in the present model (Table I).

iii) Loading and boundary conditions

The contacts between the tissues were considered as « tie » constraints. To simulate the propagation of the shear waves within the thigh segment, sinusoidal motions were prescribed to the nodes located at the surface of the skin using applied loadings in the y direction (Fig. 2B). Then, the shear wave propagation in the thigh tissues was analyzed using a two-steps process: 1) natural frequency extraction for the first 30 frequencies and 2) transient modal dynamics analysis with prescribed frequency and load during four motion cycles (0.1 ms time step) [16].

TABLE I.
CONSTITUTIVE LAWS & MECHANICAL PROPERTIES OF THE DIFFERENT TISSUES

Tissues	**Constitutive Laws & Mechanical Properties**	
	Laws	***Input values***
Skin	Non-linear hyperelastic & incompressible (Neo-Hookean): 3 layers (epidermis, dermis, hypodermis)	Density = 1 g/cm^{-3} Shear modulus: C10 = 0.55 MPa Compressibility modulus: D = 23.7 MPa^{-1} [8]
Vastus medialis muscle	Non-linear hyperelastic & incompressible (Neo-Hookean)	Shear modulus G = 32 kPa = 2C10 [9-10] Compressibility modulus D = 18 MPa^{-1} [11]
Femoral cortical Bone	Homogeneous, isotropic, linear elastic	Young's modulus: E = 7300 MPa Poisson's ratio: v = 0.3 [12] Density = 1.7 g/cm^{-3} [13]
Fat & other muscles	Isotropic and hyperelastic (Mooney-Rivlin)	C1 = 2500 Pa C2 = 1175 Pa D = 800 Pa^{-1} [14-15]

iv) Simulation of the shear wave

The impact of the MRE experimental (frequency, force) parameters and the muscle material properties (shear modulus: C_{10}) were analyzed through the simulated shear wave displacement within the vastus medialis muscle. Thus, according to the literature the frequency used in MRE soft tissue protocol was in the range of low frequency, i.e from 30Hz to 180Hz, and the applied loading from 10N to 50N. In the same way, the muscle mechanical properties (C_{10}) were also studied from 0.5 kPa to 20 kPa.

The comparison of the shear wave displacement between the different values of each parameter, within the vastus medialis, was realized with a root mean square deviation (RMSD) and a relative deviation (RD), providing a comparison in meter and in percentage, respectively. The mathematical equations are described as follows:

$$U_{RMSD} = \sqrt{\frac{\sum_i (u_{1i} - u_{2i})^2}{N}} \quad (1)$$

$$U_{RD} = \frac{U_{RMSD}}{\max(\max(u_{1i}), \max(u_{2i}))} \quad (2)$$

u_1 and u_2 are two different nodes represented the shear wave displacements along a path of N nodes located on the surface of the vastus medialis muscle.

III. RESULTS

The behavior of the shear wave propagation within a 3D finite element model of the vastus medialis muscle is

represented in Fig. 3. The shear wave is propagated and attenuated along the vastus medialis muscle with a higher amplitude close to the loading source.

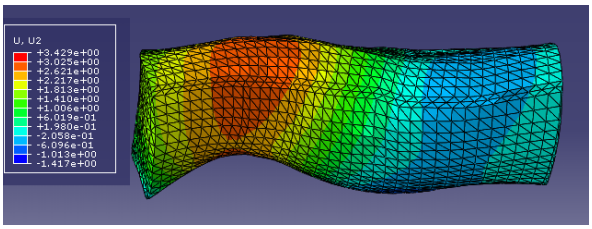

Figure 3. Pattern of the shear wave displacement within the vastus medialis muscle.

The result of the impact of the frequency values (from 30Hz to 180Hz) on the shear wave displacement within the vastus medialis is showed in Fig. 4. The important influence of the frequency parameter on the shear wave displacement is demonstrated with different wave profiles and only two sinusoidal shapes are observed for the frequencies 90Hz and 120HZ. This finding is supported by a large range of relative deviation (RD) data (e.g. 63.6% between 30Hz and 60Hz)

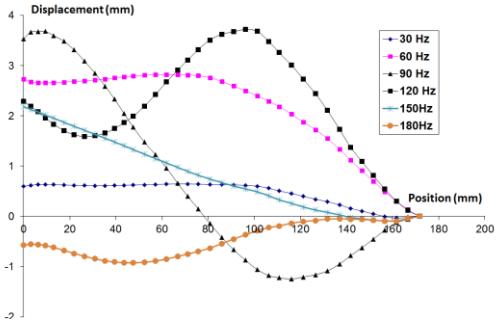

Figure 4. Superimposition of the shear wave displacement behaviors within the vastus medialis muscle for a frequency ranging from 30 Hz to 180 Hz. The curves comes from were a profile ploted along the VM muscle and the model input values were fixed with material parameters (C_{10}=16 kPa) and applied force (30 N).

The result of the influence of the applied forces, from 10 to 50N, on the shear wave displacement is represented in Fig. 5. A higher amplitude (A) of the wave is obtained when the force is increased (A_{50N} = 6mm vs A_{10N} = 1 mm). It can be noted that the three shapes of the curves are similar and the relative deviations ($U_{RD\text{-}10N\ vs\ 30N}$ = 35 %, $U_{RD\text{-}30N\ vs\ 50N}$ = 35 %) are proportional to the force.

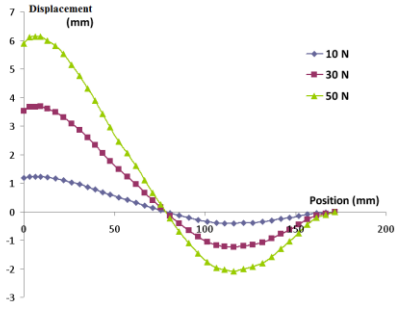

Figure 5. Effet of the boundary condition (from 10 N to 50 N) on the shear wave displacement within the vastus medialis muscle. The profiles are obtained with a fixed frequency (90 Hz) and the muscle properties set to 16 kPa (C_{10}).

It is well known that the mechanical properties of the muscle varied according to its condition. Indeed, the vastus medialis muscle in a passive state revealed lower shear modulus while in an active state the shear modulus increases with the level of contraction [17]. Thus, a large range of values (0.5 kPa < C_{10} < 20 kPa) was tested and Fig. 6 showed a sinusoidal shape for almost all the profiles. However, different amplitudes were obtained as a function of the C10 data, and the maximum relative deviation was 46%. In addition, it can be observed an increase of the wavelength with the level of the shear modulus.

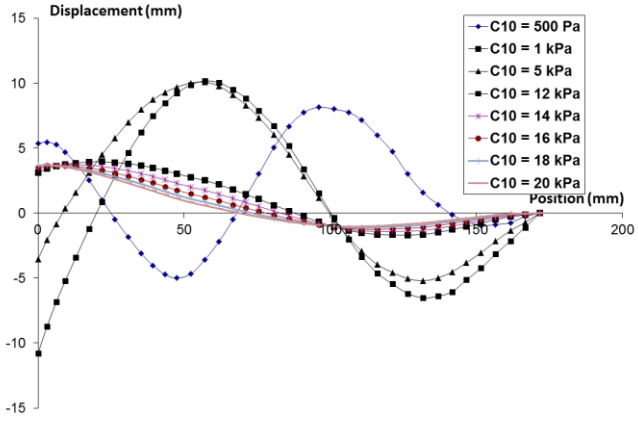

Figure 6. Superimposition of the shear wave displacement profiles for different values of the muscle mechanical properties (C_{10}: from 0.5 kPa to 20 kPa). The frequency and the applied force were fixed to 90 Hz and 30 N, respectively.

IV. Discussion

The originality of the present study is to propose a new challenging way, based on the numerical analysis of the shear wave propagation, for the development of MRE muscle protocol. To our knowledge, this work is the first to study the *in vivo* displacement of the shear wave within the vastus medialis using a 3D subject specific finite element model. In the literature, a similar *in vitro* study was performed on a phantom mimicking different tensions of the muscle fibers [16].

Finite element modeling, derived from medical image, has become an established procedure [6] for biomechanical applications. Thus, numerical models were accurately developed for biological tissues allowing the simulation of the anatomical and behavioral characteristics [18]. MRI is one of the most important medical techniques to promote for the application of finite element models in clinical practices. Moreover, finite element modeling could be also applied to MRE [16, 18]. MRE is based on the propagation of shear waves inside soft tissues and ongoing clinical protocols are under development.

Our findings showed a plausible range of frequency (from 90Hz to 120 Hz), which could be used for MRE muscle protocol in order to analyze the displacement of the shear wave within the vastus medialis muscle. This result is in agreement with the experimental frequency range used in the literature for the characterization of vastus medialis [3-

17]. Thus, the developed finite element model is able to identify the optimal range of frequency to be used during MRE tests. The boundary condition (force) is also another main experimental parameter which has a main role in the propagation of the wave. The finite element model showed expected wave displacements as a function of the level of the force. In the future, the model will be completed by the shape and the material properties of the driver [18]. This simulation is also a way to improve the development of the driver which can be adapted and optimized for the target tissue. The present study has demonstrated that the response of the shear wave displacement is linked to the set-up of experimental MRE parameters and is related to the material properties of the tissue of interest. Thanks to the present numerical approach, these different factors could be analyzed in a straightforward manner.

The finite element model revealed also different shear displacement patterns as a function of the mechanical properties of the muscle. This result suggests that the simulation of the wave propagation is sensitive to the different media. The next step will be to improve the present model in order to have similar wavelength as *in vivo* MRE measurement.

Skeletal muscle is a complex biological tissue, which has been modeled with common laws such as the hyperelastic incompressible one [9-11]. Even if the present numerical simulation provided encouraging results, more advanced muscle material laws, such as transversely isotropic hyperelastic and anisotropic materials [7, 19-20] will be implemented. Thus, the muscle fiber information (arrangement and orientation) could be taken into account in order to more accurately represent the muscle behavior through the analysis of the shear wave displacement.

Finite element modeling plays an important role in the computer-aided design [5] and the present model will be further improved for different experimental trials, leading to the set-up of optimal MRE protocol. This preliminary study opens a new direction for the development of specific MRE protocols to inaccessible tissues, such as deep muscles (i.e vastus intermedius or adductor) where the wave displacement is difficult to generate.

REFERENCES

[1] S.F. Bensamoun, G.E. Leclerc, L. Debernard, X. Cheng, L. Robert, F. Charleux, C. Rhein, J.P. Latrive. Cutoff values for alcoholic liver fibrosis using magnetic resonance elastography technique. *Alcoholism: clinical and experimental research*, 2013, 37(5), pp. 811-817.

[2] K. Riek, J.M. Millward, I. Hamann, S. Mueller, C.F. Pfueller, F. Paul J. Braun, C. Infante-Duarte, I. Sack. Magnetic resonance elastography reveals altered brain viscoelasticity in experimental autoimmune encephalomyelitis. *NeuroImage: Clinical*, 2012, 1(1), pp. 81–90.

[3] L. Debernard, G.E. Leclerc, L. Robert, F. Charleux, S.F. Bensamoun. In vivo characterization of the muscle viscoelasticity using multifrequency MR elastography (MMRE). *J Musculoskeletal Research*, 2013, 16(2), pp. 1350008-1 - 1350008-10.

[4] S.L. Ringleb, S. Bensamoun, Q. Chen, A. Manduca, R.L. Ehman, K.N. An. Applications of Magnetic Resonance Elastography to Healthy and Pathologic Skeletal Muscle. *J Magn Reson Imaging*, 2007, 25(2), pp. 301-309.

[5] D. Lacroix, J.A. Planell, P.J. Prendergast. Computer-aided design and finite-element modelling of biomaterial scaffolds for bone tissue engineering. *Phil. Trans. R. Soc. A*, 2009, 367, pp. 1993–2009.

[6] T.T. Dao, A. Rassineux, F. Charleux, M.C. Ho Ba Tho. A Robust Protocol for the Creation of Patient Specific Finite Element Models of the Musculoskeletal System from Medical Imaging Data. *Computer Methods in Biomechanics and Biomedical Engineering: Imaging & Visualization*, 2014, 1(3), pp. 138-146.

[7] T.T. Dao, S. Dakpé, P. Pouletaut, B. Devauchelle, M.C. Ho Ba Tho. Facial Mimics Simulation using MRI and Finite Element Analysis. *Proceedings of 35th Annual International Conference of the IEEE Engineering in Medicine and Biology Society*, 2013, pp. 4585-4588.

[8] H.V. Tran, F. Charleux, M. Rachik, A. Ehrlacher, M.C. Ho Ba Tho. In vivo characterization of the mechanical properties of human skin derived from MRI and indentation techniques. *Computer Methods in Biomechanics & Biomedical Engineering*, 2007, 10(6), pp. 401-407.

[9] E. Linder-Ganz, N. Shabshin, Y. Itzchak, A. Gefen. Assessment of mechanical conditions in sub-dermal tissues during sitting: A combined experimental-MRI and finite element approach. *Journal of Biomechanics*, 2007, 40(7), pp. 1443-1454.

[10] E. Linder-Ganz, N. Shabshin, A. Gefen. Patient-specific modeling of deep tissue injury biomechanics in an unconscious patient who developed myonecrosis after prolonged lying. *Journal of Tissue Viability*, 2009, 18(3), pp. 62-71.

[11] J.S. Affagard, S.F. Bensamoun, P. Feissel. Identification of the mechanical properties of the thigh muscles using a numerical example. *19th Congress of the European Society of Biomechanics*, 2013, Patras, Greece.

[12] A. Gefen, M. Megido-Ravid, Y. Itzchak, M. Arcan. Biomechanical analysis of the three-dimensional foot structure during gait: a basic tool for clinical applications. *Journal of Biomechanical Engineering*, 2000, 122, pp. 630–639.

[13] M.C. Ho Ba Tho, J.Y. Rho, R.B. Ashman. Atlas of mechanical properties of human cortical and cancellous bone, in vivo assessment of bone quality by vibration and wave propagation techniques. In: *Van der Perre G, Lowet G, Borgwardt A, editors. Leuven: Part II*, *ACCO*, 1992, pp. 7–38.

[14] M. Nazari, P. Perrier, M. Chabanas, Y. Payan. Simulation of dynamic orofacial movements using a constitutive law varying with muscle activation. *Computer Methods in Biomechanics & Biomedical Engineering*, 2010, 13(4), pp. 469–482.

[15] M. Chabanas, V. Luboz, Y. Payan. Patient specific finite element model of the face soft tissues for computer-assisted maxillofacial surgery. *Medical Image Analysis*, 2003, 7, pp. 131–151.

[16] Q. Chen, S.I. Ringleb, A. Manduca, R.L. Ehman, K.N. An. A finite element model for analyzing shear wave propagation observed in magnetic resonance elastography. *Journal of Biomechanics*, 2005, 38, pp. 2198–2203.

[17] S. Bensamoun, S.I. Ringleb, L. Littrell, Q. Chen, M. Brennan, R.L. Ehman, K.N. An. Determination of thigh muscle stiffness using magnetic resonance elastography. *J Magn Reson Imaging*, 2006, 22, pp. 242-247.

[18] G.E. Leclerc, L. Debernard, F. Foucart, L. Robert, K.M. Pelletier, F. Charleur, R.L. Ehman, M.C. Ho Ba Tho, S.F. Bensamoun. Characterization of a hyper-viscoelastic phantom mimicking biological soft tissue using an abdominal pneumatic driver with magnetic resonance elastography (MRE). *Journal of Biomechanics*, 2012, 45, pp. 952-957.

[19] M.C. Ho Ba Tho. Bone and joints modelling with individualised geometric and mechanical properties derived from medical images. *Computer Mechanics and Engineering Sciences*, 2003, 4 (3&4), pp. 489-496.

[20] J.A.C. Martins, E.B. Pires, R. Salvado, P.B. Dinis. A numerical model of passive and active behavior of skeletal muscles. *Comput. Methods Appl. Mech. Engineering*, 1998, 151, 419-433.

[21] S.S. Blemker, P.M. Pinsky, S.L. Delp. A 3D model of muscle reveals the causes of nonuniform strains in the biceps brachii. *Journal of Biomechanics*, 2005, 38, pp. 657-665.